Sensors & Transducers Journal, Vol. 5, Special Issue, March 2009, pp. 53-68

Sensors & Transducers

ISSN 1726-5479

http://www.sensorsportal.com

A Study on Dynamic Stiffening of a Rotating Beam with a Tip Mass

[1]Shengjian BAI, [2]Pinhas BEN-TZVI, [1]Qingkun ZHOU, [1]Xinsheng HUANG
[1] College of Mechatronics Engineering and Automation, National University of Defense Technology, Changsha Hunan 410073, P. R. China
[2] Department of Mechanical and Aerospace Engineering, School of Engineering and Applied Science, The George Washington University, 801 22nd St., NW, Washington, DC 20052
Tel.: (202) 994-6149
E-mail: zqkhome@gmail.com, bentzvi@gwu.edu

Received: 29 January 2009 /Accepted: 23 February 2009 /Published: 23 March 2009

Abstract: This paper presents a dynamic model of a rotating beam with a tip mass undergoing large angle, high speed maneuvering. This type of model may also be useful in modeling, analysis and development of various inertial sensors and transducers with similar operating principles. With the consideration of the second-order term of the coupling deformation field, the complete first-order approximated model (CFOAM) of a flexible spacecraft system is developed by using assumed mode method (AMM) and Lagrangian principle. A first- order approximated model (FOAM) is obtained by neglecting the high order terms of the generalized coordinates in CFOAM. A lower order simplified first-order approximated model (SFOAM) is derived by deleting the terms related to the axial deformation. Numerical simulations and theoretical analysis show that: (i) the second-order term has a significant effect on the dynamic characteristics of the system and the dynamic stiffening is accounted for, while the traditional linear approximated model (TLAM) presents invalid simulation results; (ii) the end mass has a 'stiffening' effect on the flexible system in FOAM, but a 'softening' effect in TLAM; and (iii) the SFOAM describes the dynamic behavior well and can be used for controller design.

Keywords: Flexible structure, Dynamic stiffening, Assumed mode method, Flexible beam

1. Introduction

Rotating flexible beams are used to model light robot arms, elastic linkages, helicopter rotors, satellite solar arrays, and like systems. Modeling and control of systems involving interconnected rigid structures and flexible appendages is a difficult task to accomplish, as most of these systems generally involve complex dynamics characterized by nonlinearities and strong coupling between flexible and rigid modes. Moreover, modern engineering technology is leading to ever more demanding performance criteria, such as high rotational speeds and largeangular maneuvering, increasing precision and pointing accuracy. These criteria have posed serious difficulties for all currently advocated control design methodologies. Proper dynamic modeling of the system is a foundation for further research, such as analysis of the dynamic characteristics and various controller designs.

The hybrid coordinate approach is currently the most widely used method, which describes the deformation field of flexible and rigid bodies separately. Mechanical systems undergoing high–speed rotation can produce dynamic stiffening [1, 2] due to the coupling between rigid motion and elastic deflection, and hence traditional dynamic analysis techniques are hardly applicable. The deformation field, commonly used in structural dynamics, is adopted in order to calculate the kinematics of flexible structures in the system. Therefore, modal characteristic changes due to high rotational speeds are not included in the traditional dynamic model [3].

In most cases, problems arise not because of a lack of available analytical/numerical design procedures, but because of our failure to recognize and appreciate the mechanism of dynamic stiffening. Unlike the research reported in [4,5], where the attempt was to "capture" the dynamic stiffening terms, Hong *et al* [6-8] studied the mechanism of dynamic stiffening, and concluded that the coupling deformation field can explain this phenomenon. Researches [7–10] indicated that the coupling term not included in traditional linear deformation field can have significant effect on the dynamic characteristics of the multibody system when it undergoes large rigid–body motion. The work done by Yang *et al* [7] investigated a hub–beam system by using finite element method, and pointed out that the traditional hybrid coordinate approach may lead to erroneous results in some high–speed systems. In Ref. [9], Kane's methods and the assumed mode method (AMM) were employed to investigate rigid-flexible dynamics of a spacecraft with solar panels. In this paper, we developed the complete first–order approximated model (CFOAM) of a hub–beam system by using the AMM and Lagrangian principle. The corresponding dynamic model of the tip mass is developed in a consistent manner.

This paper is organized as follows. Section 2 describes the flexible hub–beam system and defines the various symbols used. In section 3, the dynamic equations of the flexible system are developed, such as CFOAM, FOAM and SFOAM. In section 4, numerical simulations and comparisons with the traditional linear approximated model (TLAM) are presented to demonstrate the validity of the developed model (CFOAM). Furthermore, the effect of the tip mass on the dynamic characteristics of the hub–beam system is also discussed in the section. The paper concludes with a discussion provided in section 5.

2. System Description

The system shown in Fig. 1 consists of a cantilever beam B built into a rigid body H. The coordinates XY and xy in the figure are defined as the inertial frame and the reference frame, respectively. $\bar{u}_p$ is denoted as the flexible deformation vector at point P with respect to the xy frame, and $\bar{r}_A$ is the radius vector of point A on the hub. θ is considered as rigid body coordinate. After deformation, point P_0 moves to point P.

The beam is characterized by a natural length L, material properties E, ρ, and cross-sectional properties A, I, defined as follows. E and ρ are the modulus of elasticity, and the mass per unit volume of the beam, respectively. The area of the cross section is denoted by A, and the beam area moment of inertia is denoted by I.

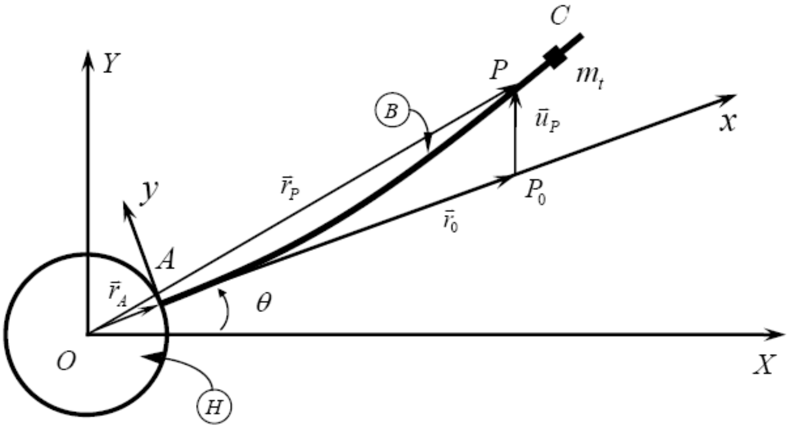

Fig. 1. Beam attached to a moving rigid hub.

3. Equations of Motion

As shown in Fig. 1, the position vector from O to P in the XY frame can be expressed as:

$$\vec{r}_p = \vec{r}_A + \vec{r}_0 + \vec{u}_p , \tag{1}$$

where $\vec{r}_A = \overline{OA}$, $\vec{r}_0 = \overline{AP_0}$, and $\vec{u}_p = \overline{P_0P}$. The coordinates of $\vec{r}_A$ and $\vec{r}_0$ in the OXY frame are represented by $\boldsymbol{r}_A$ and $\boldsymbol{r}_0$, respectively.

As shown in Fig. 2, the coordinate of the deformation vector $\vec{u}_p$ can be represented as:

$$\boldsymbol{u}_p = (u \quad v)^T = (w_1 + w_c \quad w_2)^T , \tag{2}$$

where u and v are the deform ation quantities of the point P_0 in the x and y directions in xy frame, respectively; w_1 represents the pure axial deform ation, and w_2 represents the transverse d eformation along the y–axis. w_c is the deformation associated with the foreshortening quantity due to w_2, and is represented as [7, 8]:

$$w_c = -\frac{1}{2}\int_0^x \left(\frac{\partial w_2}{\partial x}\right)^2 \mathrm{d}x \tag{3}$$

The coordinate of $\vec{r}_p$ in equation (1) may be written in the XY frame as

$$\boldsymbol{r}_p = \boldsymbol{r}_A + \mathbf{Q}(\boldsymbol{r}_0 + \boldsymbol{u}_p) = \mathbf{Q}(r_A\mathbf{e} + \boldsymbol{r}_0 + \boldsymbol{u}_p) , \tag{4}$$

where $\boldsymbol{r}_0 = (x \quad 0)^T$, $\boldsymbol{u}_p = (u \quad v)^T$, $\boldsymbol{e} = (1 \quad 0)^T$, and $\boldsymbol{r}_A = r_A(\cos\theta \quad \sin\theta)^T$. As shown in Fig. 2, the variable x is the coordinate of point P_0 in the xy frame, and the parameter $\mathbf{Q}$ is the rotational transformation matrix given by:

$$\mathbf{Q} = \begin{pmatrix} \cos\theta & -\sin\theta \\ \sin\theta & \cos\theta \end{pmatrix}, \tag{5}$$

where θ is the angular displacement of the hub.

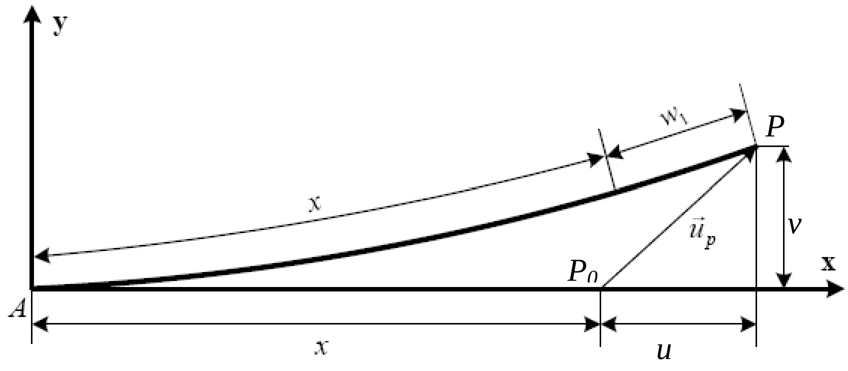

Fig. 2. Description of the beam deformation.

The first-order derivative of $\boldsymbol{r}_P$ may be expressed as

$$\dot{\boldsymbol{r}}_P = \mathbf{QI}(r_A\mathbf{e} + \boldsymbol{r}_0 + \boldsymbol{u}_p)\dot{\theta} + \mathbf{Q}\dot{\boldsymbol{u}}_p \tag{6}$$

where

$$\mathbf{I} = \begin{pmatrix} 0 & -1 \\ 1 & 0 \end{pmatrix}, \qquad \dot{\boldsymbol{u}}_p = \begin{pmatrix} \dot{w}_1 - \dot{w}_c \\ \dot{w}_2 \end{pmatrix}. \tag{7}$$

From Eq. (6), we can derive

$$\dot{\boldsymbol{r}}_P^T\dot{\boldsymbol{r}}_P = \dot{\theta}^2\left\{(r_A + w_1 + w_c + x)^2 + w_2^2\right\} + (\dot{w}_1 + \dot{w}_c)^2 + \dot{w}_2^2 + 2\dot{\theta}\left\{(r_A + w_1 + w_c + x)\dot{w}_2 - (\dot{w}_1 + \dot{w}_c)v\right\} \tag{8}$$

The kinetic energy of the hub–beam system is written as

$$T = T_h + T_b + T_t = \frac{1}{2}J_h\dot{\theta}^2 + \frac{1}{2}\int_0^L \dot{\boldsymbol{r}}_P^T\dot{\boldsymbol{r}}_P dx + \frac{1}{2}\boldsymbol{m}_t\dot{\boldsymbol{r}}_m^T\dot{\boldsymbol{r}}_m, \tag{9}$$

where T_h , T_b and T_t are the kinetic energy of the hub, beam and tip m ass, respectively. J_h is the rotational inertia of the hub. m_t is the weight of the tip mass, r_m is the coordinate of the position vector from O to the tip mass.

By using Euler–Bernoulli theory, the potential energy is given by

$$U = \frac{1}{2}\int_0^L EA\left(\frac{\partial w_1}{\partial x}\right)^2 dx + \frac{1}{2}\int_0^L EI\left(\frac{\partial^2 w_2}{\partial x^2}\right)^2 dx \tag{10}$$

where E is Young's modulus, A is the cross–sectional area and I is the area moment of inertia. The AMM is used to discretize the elastic beam, then the deformations u and v can be represented as:

$$u(x,t) = \sum_{i=1}^n f_i^{(1)}(x)q_i^{(1)}(t), \quad v(x,t) = \sum_{i=1}^n f_i^{(2)}(x)q_i^{(2)}(t), \tag{11}$$

where $f_i^{(1)}(x)$ and $f_i^{(2)}(x)$ are the adm issible functions, $q_i^{(1)}(t)$ and $q_i^{(2)}(t)$ are the mode generalized coordinates, and n refers to the num ber of included modes. In subsequent derivations, $\boldsymbol{f}_1(x)$, $\boldsymbol{f}_2(x)$, $\boldsymbol{q}_1(t)$ and $\boldsymbol{q}_2(t)$ are adopted to represent the vectors of $f_i^{(1)}(x)$, $f_i^{(2)}(x)$, $q_i^{(1)}(t)$ and $q_i^{(2)}(t)$ respectively. From Eq. (11), Eq. (8) can be rewritten as

$$\begin{aligned}\dot{\boldsymbol{r}}_p^T\dot{\boldsymbol{r}}_p &= \dot{\theta}^2\left\{(r_A+x)^2+2(r_A+x)\boldsymbol{f}_1\boldsymbol{q}_1-(r_A+x)\boldsymbol{q}_2^T\boldsymbol{S}\boldsymbol{q}_2+\boldsymbol{q}_1^T\boldsymbol{f}_1^T\boldsymbol{f}_1\boldsymbol{q}_1+\boldsymbol{q}_2^T\boldsymbol{f}_2^T\boldsymbol{f}_2\boldsymbol{q}_2-\boldsymbol{f}_1\boldsymbol{q}_1\boldsymbol{q}_2^T\boldsymbol{S}\boldsymbol{q}_2+\frac{1}{4}\left(\boldsymbol{q}_2^T\boldsymbol{S}\boldsymbol{q}_2\right)^2\right\} \\ &+2\dot{\theta}\left\{(r_o+x)\boldsymbol{f}_2\dot{\boldsymbol{q}}_2+\boldsymbol{q}_1^T\boldsymbol{f}_1^T\boldsymbol{f}_2\dot{\boldsymbol{q}}_2-\boldsymbol{q}_2^T\boldsymbol{f}_2^T\boldsymbol{f}_1\dot{\boldsymbol{q}}_1+\boldsymbol{q}_2^T\boldsymbol{S}\dot{\boldsymbol{q}}_2\boldsymbol{f}_2\boldsymbol{q}_2\right\}+\dot{\boldsymbol{q}}_1^T\boldsymbol{f}_1^T\boldsymbol{f}_1\dot{\boldsymbol{q}}_1+\dot{\boldsymbol{q}}_2^T\boldsymbol{f}_2^T\boldsymbol{f}_2\dot{\boldsymbol{q}}_2-2\dot{\boldsymbol{q}}_1^T\boldsymbol{f}_1^T\boldsymbol{q}_2^T\boldsymbol{S}\dot{\boldsymbol{q}}_2+\left(\boldsymbol{q}_2^T\boldsymbol{S}\dot{\boldsymbol{q}}_2\right)^2\end{aligned}, \quad (12)$$

where $\dot{\theta}^2\boldsymbol{f}_1\boldsymbol{q}_1\boldsymbol{q}_2^T\boldsymbol{S}\boldsymbol{q}_2$, $2\dot{\theta}\boldsymbol{q}_2^T\boldsymbol{S}\dot{\boldsymbol{q}}_2\boldsymbol{f}_2\boldsymbol{q}_2$, $2\dot{\boldsymbol{q}}_1^T\boldsymbol{f}_1^T\boldsymbol{q}_2^T\boldsymbol{S}\dot{\boldsymbol{q}}_2$, $\left(\boldsymbol{q}_2^T\boldsymbol{S}\dot{\boldsymbol{q}}_2\right)^2$ and $\frac{1}{4}\dot{\theta}^2\left(\boldsymbol{q}_2^T\boldsymbol{S}\boldsymbol{q}_2\right)^2$ are high order terms related to the generalized coordinates.

3.1. Equations of Motion at the Element Level

To derive the equations of m otion in a m ore co mpact form, the follo wing elem ent coefficie nts and matrices are introduced:

$$J_b = \int_0^L \rho A(r_A+x)^2\,dx \quad (13)$$

$$\boldsymbol{K}_1 = \int_0^L EA\left(\frac{\partial \boldsymbol{f}_1(x)}{\partial x}\right)^T\frac{\partial \boldsymbol{f}_1(x)}{\partial x}dx \quad (14)$$

$$\boldsymbol{K}_2 = \int_0^L EI\left(\frac{\partial^2 \boldsymbol{f}_2(x)}{\partial x^2}\right)^T\frac{\partial^2 \boldsymbol{f}_2(x)}{\partial x^2}dx \quad (15)$$

$$\boldsymbol{M}_i = \int_0^L \rho A\boldsymbol{f}_i^T\boldsymbol{f}_i dx, \qquad i=1,2 \quad (16)$$

$$\boldsymbol{V}_i = \int_0^L \rho A(r_A+x)\boldsymbol{f}_i dx \qquad i=1,2 \quad (17)$$

$$\boldsymbol{D} = \int_0^L \rho A(r_A+x)\boldsymbol{S}(x)\,dx \quad (18)$$

$$\boldsymbol{R} = \int_0^L \rho A\boldsymbol{f}_1^T\boldsymbol{f}_2 dx\,, \quad (19)$$

where J_b is the rotational inertia of the beam about the hub center, matrices $\boldsymbol{K}_1 \in R^{n\times n}$ and $\boldsymbol{K}_2 \in R^{n\times n}$ are the conv entional s tiffness m atrices, $\boldsymbol{M}_i \in R^{n\times n}, i=1,2$ are g eneralized elastic m ass m atrices, m atrix $\boldsymbol{D}$ results from the second orde r term of the coupling defo rmation field (3), m atrix $\boldsymbol{R}$ results f rom the gyroscopic effects, and $\boldsymbol{S}(x)$ results from w_c and is represented as:

$$\boldsymbol{S}(x) = \int_0^x \frac{\partial \boldsymbol{f}_2^T(\xi)}{\partial \xi}\frac{\partial \boldsymbol{f}_2(\xi)}{\partial \xi}\mathrm{d}\xi \quad (20)$$

It is im portant to note th at m atrix $\boldsymbol{D}$ is non-negative definite because $\boldsymbol{S}(x)$ is a non-negative definite matrix.

Using AMM with n assumed modes, Eqs. (9) and (10) can be rewritten as:

$$
\begin{aligned}
T = \dot{\theta}^2\left(\frac{1}{2}J_h + \frac{1}{2}J_b + \boldsymbol{V}_1\boldsymbol{q}_1 + \frac{1}{2}\boldsymbol{q}_1^T\boldsymbol{M}_1\boldsymbol{q}_1 + \frac{1}{2}\boldsymbol{q}_2^T\boldsymbol{M}_2\boldsymbol{q}_2 - \frac{1}{2}\boldsymbol{q}_2^T\boldsymbol{D}\boldsymbol{q}_2\right) + \dot{\theta}\left(\boldsymbol{V}_2\dot{\boldsymbol{q}}_2 + \boldsymbol{q}_1^T\boldsymbol{R}\dot{\boldsymbol{q}}_2 - \boldsymbol{q}_2^T\boldsymbol{R}^T\dot{\boldsymbol{q}}_1\right) + \frac{1}{2}\dot{\boldsymbol{q}}_1^T\boldsymbol{M}_1\dot{\boldsymbol{q}}_1 \\
+ \frac{1}{2}\dot{\boldsymbol{q}}_2^T\boldsymbol{M}_2\dot{\boldsymbol{q}}_2 + \int_0^L \rho A\left\{\left(\boldsymbol{q}_2^T\boldsymbol{S}\dot{\boldsymbol{q}}_2\right)^2 - \dot{\theta}^2\boldsymbol{f}_1\boldsymbol{q}_1\boldsymbol{q}_2^T\boldsymbol{S}\boldsymbol{q}_2 + \frac{1}{4}\dot{\theta}^2\left(\boldsymbol{q}_2^T\boldsymbol{S}\boldsymbol{q}_2\right)^2 + 2\dot{\theta}\boldsymbol{q}_2^T\boldsymbol{S}\dot{\boldsymbol{q}}_2\boldsymbol{f}_2\boldsymbol{q}_2 - 2\boldsymbol{f}_1\dot{\boldsymbol{q}}_1\boldsymbol{q}_2^T\boldsymbol{S}\dot{\boldsymbol{q}}_2\right\}dx
\end{aligned}
\tag{21}
$$

$$
U = \frac{1}{2}\boldsymbol{q}_1^T\boldsymbol{K}_1\boldsymbol{q}_1 + \frac{1}{2}\boldsymbol{q}_2^T\boldsymbol{K}_2\boldsymbol{q}_2 \tag{22}
$$

The governing equations of motion can now be obtained through the application of the Lagrangian principle

$$
\frac{d}{dt}\left(\frac{\partial T}{\partial \hbar_i}\right) - \frac{\partial T}{\partial h_i} + \frac{\partial U}{\partial h_i} = Q_i \qquad i = 1, 2, \cdots, n+1, \tag{23}
$$

where η_i are the system generalized coordinates, and Q_i the non-conservative generalized forces due to environmental effects and actuators.

By substituting Eqs. (21) and (22) into Eq.(23), the equations of motion of the flexible system at the element level in compact form can be written as:

$$
\begin{bmatrix} M_{\theta\theta} & \boldsymbol{M}_{\theta q_1} & \boldsymbol{M}_{\theta q_2} \\ \boldsymbol{M}_{q_1\theta} & \boldsymbol{M}_{q_1q_1} & \boldsymbol{0} \\ \boldsymbol{M}_{q_2\theta} & \boldsymbol{0} & \boldsymbol{M}_{q_2q_2} \end{bmatrix}
\begin{bmatrix} \ddot{\theta} \\ \ddot{\boldsymbol{q}}_1 \\ \ddot{\boldsymbol{q}}_2 \end{bmatrix}
+ 2\dot{\theta}
\begin{bmatrix} 0 & \boldsymbol{0} & \boldsymbol{0} \\ 0 & \boldsymbol{0} & \boldsymbol{G}_{q_1q_2} \\ 0 & \boldsymbol{G}_{q_2q_1} & \boldsymbol{0} \end{bmatrix}
\begin{bmatrix} \dot{\theta} \\ \dot{\boldsymbol{q}}_1 \\ \dot{\boldsymbol{q}}_2 \end{bmatrix}
+
\begin{bmatrix} 0 & \boldsymbol{0} & \boldsymbol{0} \\ 0 & \boldsymbol{K}_{q_1q_1} & \boldsymbol{0} \\ 0 & \boldsymbol{0} & \boldsymbol{K}_{q_2q_2} \end{bmatrix}
\begin{bmatrix} \theta \\ \boldsymbol{q}_1 \\ \boldsymbol{q}_2 \end{bmatrix}
=
\begin{bmatrix} Q_\theta \\ \boldsymbol{Q}_{q_1} \\ \boldsymbol{Q}_{q_2} \end{bmatrix}
+
\begin{bmatrix} \tau \\ \boldsymbol{0} \\ \boldsymbol{0} \end{bmatrix}, \tag{24}
$$

where $\boldsymbol{M}_{\theta\theta} \in R^1$ is the rotary inertia of the system, $\boldsymbol{M}_{q_1q_1} \in R^{n\times n}$ and $\boldsymbol{M}_{q_2q_2} \in R^{n\times n}$ are the beam generalized elastic mass matrices, $\boldsymbol{M}_{\theta q_1} \in R^{1\times n}$, $\boldsymbol{M}_{\theta q_2} \in R^{1\times n}$, $\boldsymbol{M}_{q_1\theta} \in R^{n\times 1}$ and $\boldsymbol{M}_{q_2\theta} \in R^{n\times 1}$ represent the non linear inertia coupling between the motion of the reference frame and the elastic deformations, $\boldsymbol{K}_{q_1q_1} \in R^{n\times n}$ and $\boldsymbol{K}_{q_2q_2} \in R^{n\times n}$ are generalized elastic stiffness matrices that are shown to be affected by both the motion of the reference frame and the elastic deformations, Q_θ represents inertia forces, and τ is the rotational external torque. The parameters in Eq. (24) are given as follows:

$$
M_{\theta\theta} = J_h + J_b + \boldsymbol{q}_1^T\boldsymbol{M}_1\boldsymbol{q}_1 + \boldsymbol{q}_2^T\boldsymbol{M}_2\boldsymbol{q}_2 + 2\boldsymbol{V}_{11}\boldsymbol{q}_1 - \underline{\boldsymbol{q}_2^T\boldsymbol{D}\boldsymbol{q}_2} + \Delta M_{\theta\theta} \tag{25}
$$

$$
\boldsymbol{M}_{q_1\theta} = \boldsymbol{M}_{\theta q_1}^T = -\boldsymbol{R}\boldsymbol{q}_2 \tag{26}
$$

$$
\boldsymbol{M}_{\theta q_2} = \boldsymbol{M}_{q_2\theta}^T = \boldsymbol{V}_{12} + \boldsymbol{q}_1^T\boldsymbol{R} + \Delta\boldsymbol{M}_{q_2\theta}^T \tag{27}
$$

$$
\boldsymbol{M}_{\theta q_2} = \boldsymbol{M}_{q_2\theta}^T = \boldsymbol{V}_{12} + \boldsymbol{q}_1^T\boldsymbol{R} + \Delta\boldsymbol{M}_{q_2\theta}^T \tag{28}
$$

$$
\boldsymbol{G}_{q_1q_2} = -\boldsymbol{G}_{q_2q_1}^T = -\boldsymbol{R} \tag{29}
$$

$$
\boldsymbol{K}_{q_1q_1} = \boldsymbol{K}_1 - \dot{\theta}^2\boldsymbol{M}_1 \tag{30}
$$

$$
\boldsymbol{K}_{q_2q_2} = \boldsymbol{K}_2 - \dot{\theta}^2\boldsymbol{M}_2 + \underline{\dot{\theta}^2\boldsymbol{D}} \tag{31}
$$

$$Q_{\theta} = -2\dot{\theta}\left[\left(\boldsymbol{q}_1^T \boldsymbol{M}_1 \dot{\boldsymbol{q}}_1 + \boldsymbol{q}_2^T \boldsymbol{M}_2 \dot{\boldsymbol{q}}_2\right) + \boldsymbol{V}_1 \dot{\boldsymbol{q}}_1 - \underline{\boldsymbol{q}_2^T \boldsymbol{D} \dot{\boldsymbol{q}}_2}\right] + \Delta Q_{\theta} \tag{32}$$

$$\boldsymbol{Q}_{q_1} = \dot{\theta}^2 \boldsymbol{V}_1^T + \Delta \boldsymbol{Q}_{q_1} \tag{33}$$

$$\boldsymbol{Q}_{q_2} = \Delta \boldsymbol{Q}_{q_2}, \tag{34}$$

where

$$\Delta M_{\theta\theta} = \int_0^L \rho A \left\{ \frac{1}{2}\left(\boldsymbol{q}_2^T \boldsymbol{S} \boldsymbol{q}_2\right)^2 - 2\boldsymbol{f}_1 \boldsymbol{q}_1 \boldsymbol{q}_2^T \boldsymbol{S} \boldsymbol{q}_2 \right\} dx \tag{35}$$

$$\Delta \boldsymbol{M}_{q_2\theta} = 4\int_0^L \rho A \boldsymbol{f}_2 \boldsymbol{q}_2 \boldsymbol{S} \boldsymbol{q}_2 dx \tag{36}$$

$$\Delta Q_{\theta} = 2\int_0^L \rho A \left\{ -\boldsymbol{f}_1 \dot{\boldsymbol{q}}_1 \boldsymbol{q}_2^T \boldsymbol{S} \boldsymbol{q}_2 \dot{\theta} + \left(\boldsymbol{q}_2^T \boldsymbol{S} \boldsymbol{q}_2\right)\left(\boldsymbol{q}_2^T \boldsymbol{S} \dot{\boldsymbol{q}}_2\right)\dot{\theta} - 2\boldsymbol{f}_1 \boldsymbol{q}_1 \boldsymbol{q}_2^T \boldsymbol{S} \dot{\boldsymbol{q}}_2 \dot{\theta} + \dot{\boldsymbol{q}}_2^T \boldsymbol{S} \dot{\boldsymbol{q}}_2 \boldsymbol{f}_2 \boldsymbol{q}_2 + \boldsymbol{q}_2^T \boldsymbol{S} \ddot{\boldsymbol{q}}_2 \boldsymbol{f}_2 \boldsymbol{q}_2 + \boldsymbol{q}_2^T \boldsymbol{S} \dot{\boldsymbol{q}}_2 \boldsymbol{f}_2 \dot{\boldsymbol{q}}_2 \right\} dx \tag{37}$$

$$\Delta \boldsymbol{Q}_{q_1} = -\int_0^L \rho A \left\{ 2\boldsymbol{f}_1^T \dot{\boldsymbol{q}}_2^T \boldsymbol{S} \dot{\boldsymbol{q}}_2 + 2\boldsymbol{f}_1^T \boldsymbol{q}_2^T \boldsymbol{S} \ddot{\boldsymbol{q}}_2 + \dot{\theta}^2 \boldsymbol{f}_1^T \boldsymbol{q}_2^T \boldsymbol{S} \boldsymbol{q}_2 \right\} dx \tag{38}$$

$$\begin{aligned} \Delta \boldsymbol{Q}_{q_2} = \int_0^L \rho A \{ & 2\dot{\theta} \boldsymbol{f}_2 \dot{\boldsymbol{q}}_2 \boldsymbol{S} \boldsymbol{q}_2 + 2\dot{\theta} \boldsymbol{f}_2 \boldsymbol{q}_2 \boldsymbol{S} \dot{\boldsymbol{q}}_2 - 2\boldsymbol{f}_1 \ddot{\boldsymbol{q}}_1 \boldsymbol{S} \boldsymbol{q}_2 - 2\boldsymbol{f}_1 \dot{\boldsymbol{q}}_1 \boldsymbol{S} \dot{\boldsymbol{q}}_2 + 2\dot{\boldsymbol{q}}_2^T \boldsymbol{S} \dot{\boldsymbol{q}}_2 \boldsymbol{S} \boldsymbol{q}_2 + 2\dot{\theta} \boldsymbol{q}_2^T \boldsymbol{S} \dot{\boldsymbol{q}}_2 \boldsymbol{f}_2^T + 2\dot{\theta} \boldsymbol{f}_2 \boldsymbol{q}_2 \boldsymbol{S} \dot{\boldsymbol{q}}_2 \\ & + 2\boldsymbol{q}_2^T \boldsymbol{S} \ddot{\boldsymbol{q}}_2 \boldsymbol{S} \boldsymbol{q}_2 + 2\boldsymbol{q}_2^T \boldsymbol{S} \dot{\boldsymbol{q}}_2 \boldsymbol{S} \dot{\boldsymbol{q}}_2 - 2\boldsymbol{f}_1 \boldsymbol{q}_1 \boldsymbol{S} \boldsymbol{q}_2 \dot{\theta}^2 + \boldsymbol{q}_2^T \boldsymbol{S} \boldsymbol{q}_2 \boldsymbol{S} \boldsymbol{q}_2 \dot{\theta}^2 - 2\boldsymbol{f}_1 \dot{\boldsymbol{q}}_1 \boldsymbol{S} \dot{\boldsymbol{q}}_2 + 2\left(\boldsymbol{q}_2^T \boldsymbol{S} \dot{\boldsymbol{q}}_2\right) \boldsymbol{S} \dot{\boldsymbol{q}}_2 \} dx \end{aligned} \tag{39}$$

Equations (35)-(39) are derived from the high order terms in Eq. (12).

In Eq. (24), the nonlinear coupling between the rigid–body motion and the elastic deformations can be easily seen. The underlined terms in Eqs. (25), (31) and (32) result from the coupling deformation field. The newly established Eqs. (24)-(34) are called the complete first-order approximate model(CFOAM), while the CFOAM without Eqs.(35)-(39) are called the first-order approximate model (FOAM). The FOAM without the underlined terms are called traditional linear approximate model (TLAM). A simplified first-order approximate model (SFOAM) of the hub-beam system can be derived from FOAM by deleting the elements related to Q_{θ}, $\boldsymbol{q}_1$ and $\dot{\boldsymbol{q}}_1$:

$$\begin{bmatrix} M_{\theta\theta} & \boldsymbol{M}_{\theta q_2} \\ \boldsymbol{M}_{q_2\theta} & \boldsymbol{M}_{q_2 q_2} \end{bmatrix} \begin{bmatrix} \ddot{\theta} \\ \ddot{\boldsymbol{q}}_2 \end{bmatrix} + \begin{bmatrix} 0 & \boldsymbol{0} \\ \boldsymbol{0} & \boldsymbol{K}_{q_2 q_2} \end{bmatrix} \begin{bmatrix} \theta \\ \boldsymbol{q}_2 \end{bmatrix} = \begin{bmatrix} \tau \\ \boldsymbol{0} \end{bmatrix}, \tag{40}$$

where $M_{\theta\theta}, \boldsymbol{M}_{\theta q_2}, \boldsymbol{M}_{q_2\theta}, \boldsymbol{M}_{q_2 q_2}$ and $\boldsymbol{K}_{q_2 q_2}$ can also be obtained by deleting the elements related to $\boldsymbol{q}_1$ and $\dot{\boldsymbol{q}}_1$ in (25), (27), (28), (31) and(32). It is noted that SFOAM can be used for controller design.

3.2. Tip Mass Dynamics

The tip mass, as shown in Fig.1, is located at a distance l along the undeformed beam from point A. It is considered to have a mass m_t. The position vector of the tip mass with respect to the inertial frame XY can be represented as

$$\boldsymbol{r}_m = \boldsymbol{r}_A + \mathbf{Q}(\boldsymbol{r}_t + \boldsymbol{u}_t), \tag{41}$$

where $\boldsymbol{r}_t = (l \quad 0)^T$ is the position vector of the tip mass in the reference frame xy in the undeformed configuration, and $\boldsymbol{u}_t$ is the elastic displacement vector of the point on the beam to which the tip mass is attached.

The contribution of the tip mass to FOAM of the multibody system can also be included by applying the Lagrangian principle. The equations can be represented by the following matrix form:

$$\begin{bmatrix} M^{l}_{\theta\theta} & \boldsymbol{M}^{l}_{\theta q_1} & \boldsymbol{M}^{l}_{\theta q_2} \\ \boldsymbol{M}^{l}_{q_1\theta} & \boldsymbol{M}^{l}_{q_1 q_1} & \boldsymbol{0} \\ \boldsymbol{M}^{l}_{q_2\theta} & \boldsymbol{0} & \boldsymbol{M}^{l}_{q_2 q_2} \end{bmatrix} \begin{bmatrix} \ddot{\theta} \\ \ddot{\boldsymbol{q}}_1 \\ \ddot{\boldsymbol{q}}_2 \end{bmatrix} + 2\dot{\theta} \begin{bmatrix} 0 & \boldsymbol{0} & \boldsymbol{0} \\ \boldsymbol{0} & \boldsymbol{0} & \boldsymbol{G}^{l}_{q_1 q_2} \\ \boldsymbol{0} & \boldsymbol{G}^{l}_{q_2 q_1} & \boldsymbol{0} \end{bmatrix} \begin{bmatrix} \dot{\theta} \\ \dot{\boldsymbol{q}}_1 \\ \dot{\boldsymbol{q}}_2 \end{bmatrix} + \begin{bmatrix} 0 & \boldsymbol{0} & \boldsymbol{0} \\ \boldsymbol{0} & \boldsymbol{K}^{l}_{q_1 q_1} & \boldsymbol{0} \\ \boldsymbol{0} & \boldsymbol{0} & \boldsymbol{K}^{l}_{q_2 q_2} \end{bmatrix} \begin{bmatrix} \theta \\ \boldsymbol{q}_1 \\ \boldsymbol{q}_2 \end{bmatrix} = \begin{bmatrix} Q^{l}_{\theta} \\ \boldsymbol{Q}^{l}_{q_1} \\ \boldsymbol{0} \end{bmatrix}, \tag{42}$$

where the coefficients and matrices are shown in the appendix.

3.3. Equations of Motion of the Whole System

The FOAM of the whole system can be obtained from Eqs. (24) and (42) directly by adding the corresponding entries of the generalized matrices. Two different models are developed in order to examine the effect of the second order term. The established equations with and without the underlined terms are called FOAM and TLAM, respectively.

4. Simulations and Results

The physical parameters of the flexible hub-beam system are shown in Table 1. The payload is represented by a point mass m_t at the free end of the beam. The number of included modes n is 5.

Table 1. Physical parameters.

Property	Symbol	Value
Beam length	L	8m
Mass per unit volume	ρ	2.7667×103 kg/m^3
Cross-Section	A	7.2968×10-5 m^2
Young's modulus	E	6.8952×1010 N/m^2
Beam area moment of inertia	I	8.2189×10-9m^4
Hub moment of inertia	J_h	200 kgm^2
Hub radius	r	0.5 m
Tip mass	m_t	0.1 kg

The response of the flexible motion is simulated by assuming that the slewing motion follows a prescribed trajectory, and the maneuver profile [2] is given by

$$\dot{\theta} = \begin{cases} \dfrac{w_f}{t_f} - \dfrac{w_f}{2\pi}\sin\left(\dfrac{2\pi}{t_f}t\right), & 0 \le t \le t_f \\ w_f\,, & t > t_f \end{cases} \tag{43}$$

where w_f and t_f represent the velocity of the hub at the end of the maneuver, and the time to reach the maximum velocity, respectively.

4.1. Vibration Response of CFOAM and FOAM

Let us consider first CFOAM and FOAM of the hub–beam system without a tip mass.

The terms (35)-(39) in CFOAM are the integrations of the generalized coordinates. Thus, CFOAM is not only complicated in presentation, but also difficult in symbolic computation and numerical simulation. Fig. 3 shows the simulation results with the neglected terms when w_f is 3 rad/s. For simplicity, the first mode is taken into account. In fact, it dominates the transverse response of the beam (see Fig. 6). We can see from Fig. 3 that these terms have small amplitude and tend to reach zero after 30 s.

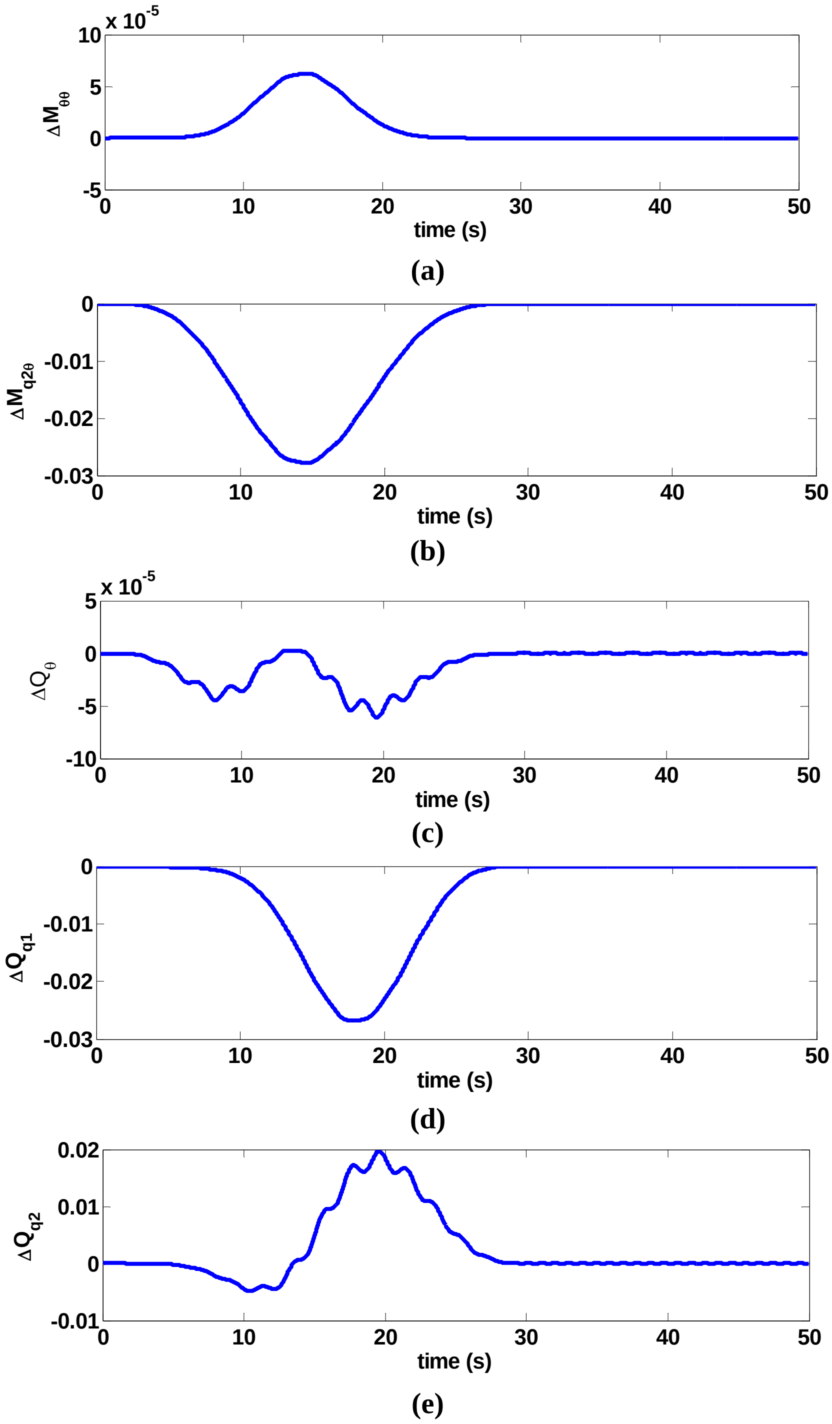

Fig. 3. Response with the neglected terms when w_f =3 rad/s.

Fig. 4 shows that the displacement of CFOAM and FOAM is exactly the same. This confirms that the simplification is valid and FOAM can be used to investigate the dynamic characteristics of the flexible multibody system.

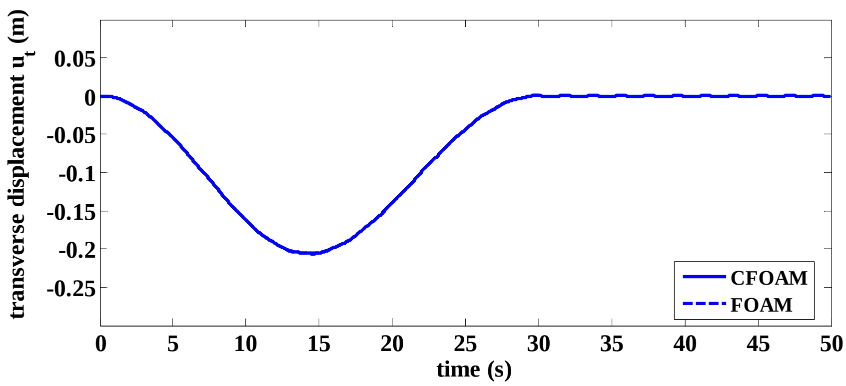

Fig. 4. Tip displacement of CFOAM and FOAM when w_f =3 rad/s.

4.2. Vibration Response of FOAM and TLAM

Fig. 5 shows the simulation results of TLAM and FOAM for comparison. It can be seen that the vibration response of the flexible beam diverges when the angular velocity is greater than 3rad/s. It should be noted that the resulting tip displacement of TLAM has exceeded the assumption of small deformations. When the angular velocity is smaller than 3rad/s but close to the critical value, e.g., 2.8rad/s, the maximum tip deflection of TLAM is much larger than that of FOAM, which are approximately 0.49m and 0.22m, respectively. Moreover, the residual vibration amplitude of TLAM is approximately 100 times larger than that of FOAM. It can be concluded therefore that TLAM is invalid for describing the deformation of multibody systems in high–speed cases.

Because the second order term in the defomation is not included, the generalized elastic stiffness matrix in the TLAM is expressed as $\boldsymbol{K}_{q_2q_2} = \boldsymbol{K}_2 - \dot{\theta}^2\boldsymbol{M}_2$. From this expression, it is seen that the stiffness matrix may be negative definite when the angular velocity surpasses a critical value. In fact, it can be calculated from Eq. (31) that the critical angularvelocity is 2.91rad/s. This is thefirst order natural circle frequency of the beam according to Table 2. The frequencies evaluated with TLAM are 'sofening' compared to the natural frequencies. On the other hand, the generalized elastic stiffness matrix in FOAM is expressed as $\boldsymbol{K}_{q_2q_2} = \boldsymbol{K}_2 - \dot{\theta}^2\boldsymbol{M}_2 + \underline{\dot{\theta}^2\boldsymbol{D}}$, in which the underlined term $\dot{\theta}^2\boldsymbol{D}$ is non–negative definite, and can make $\boldsymbol{K}_{q_2q_2}$ definite positive.

As shown in Table 2, the natural vibration frequency is larger than that evaluated with TLAM, but less than that evaluated with FOAM, i.e. the second order term in coupling deformation field has a 'stiffening' effect on the frequencies of the multibody system in high-speed case. The difference values become larger when the speed increases.

Table 2. The inertia force under different torques.

Mode order	**1**	**2**	**3**	**4**	**5**
Natural frequency	0.4635	2.9047	8.1332	15.9377	26.3462
TLAM (1 rad/s)	0.4353	2.9003	8.1316	15.9369	26.3457
FOAM (1 rad/s)	0.4714	2.9308	8.1618	15.9682	26.3776

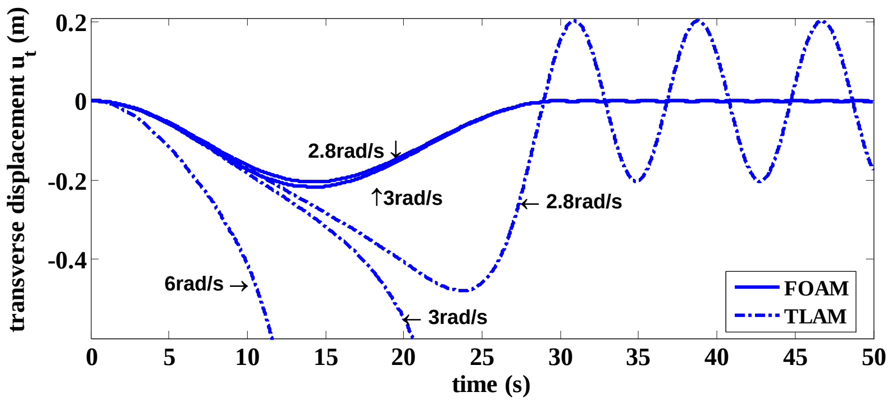

(a) Transverse response of the tip of the beam.

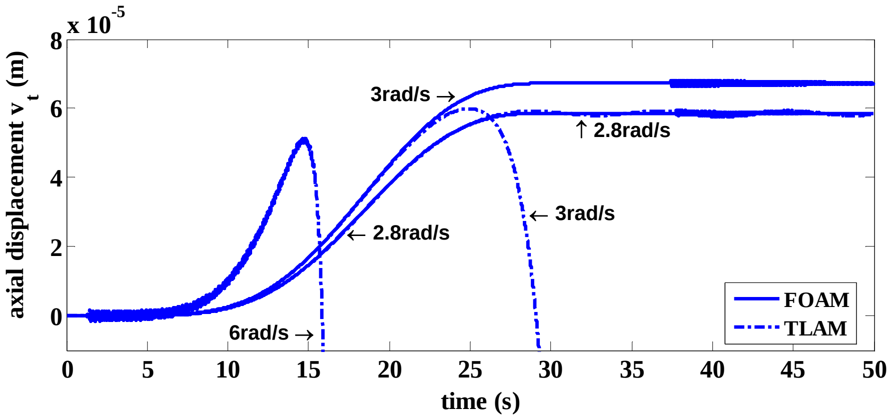

(b) Axial response of the tip of the beam.

Fig. 5. Beam vibration response with respect to different angular velocities.

4.3. Vibration Response of FOAM and SFOAM

Consider first FOAM of the hub–beam system without tip mass. For $w_f = 5rad/s$, and $t_f = 30s$, the resulting response of the first five modes of the flexible hub–beam system is shown in Fig. 6.

It can be seen that the peak response of the transverse displacement is approximately 1500 times larger than that of the axial displacement. As shown in Fig. 6a, the response of the first two modes dominates over the response of the higher modes. Thus the elements related to $\boldsymbol{q}_1$ and $\dot{\boldsymbol{q}}_1$ in (25) can be neglected for simplification. Fig. 6b clearly shows that the simulation results for the different number of modes are exactly the same.

Next, we assume that the torque acting on the rigid hub has the following profile:

$$\tau(t) = \begin{cases} \tau_m \sin\left(\dfrac{2\pi}{T}t\right), & 0 \le t \le t_f \\ 0, & t > t_f \end{cases}, \tag{44}$$

where $t_f = 10s$ is the maneuver time, and τ_m is the maximum torque.

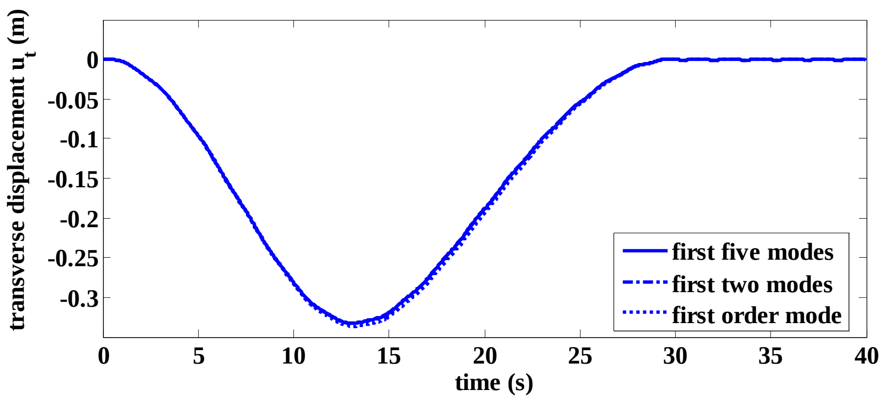

(a) Response of the transverse displacement.

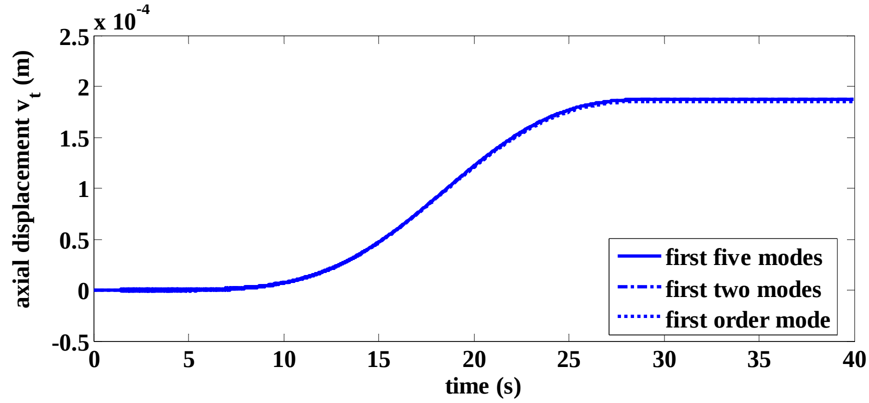

(b) Response of the axial displacement.

Fig. 6. Beam vibration response to prescribed slew maneuver.

As shown in Fig. 7, the maximum amplitude of Q_θ is 2.62 N m, which is about 6.5 % of τ_m. Table 3 outlines the maximum amplitudes of the generated Q_θ with different $\tau(t)$ acting on the hub. It is clear that Q_θ is small and hence can be treated as a small disturbance of $\tau(t)$. Therefore, for simplification, it is not included in SFOAM.

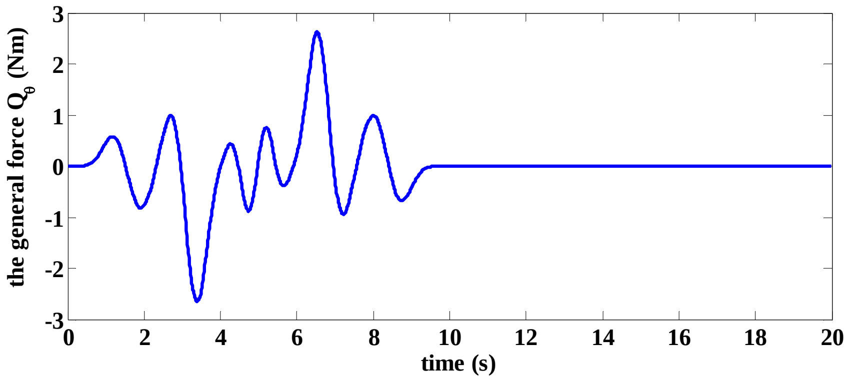

Fig. 7. Response of Q_θ when τ_m is 400Nm.

Table 3. The first five vibration frequencies (Hz).

Torque	Value (Nm)			
τ_m	50.0	100	200	400
Q_θ	6.24×10^{-3}	4.61×10^{-2}	3.72×10^{-2}	2.62

Fig. 8 shows the simulation results of FADM and SFOAM. When the torque is small (50 Nm), as shown in Fig. 8 a, the simulation curves of SFADM almost coincided with that of FOAM. But the difference appears when τ_m is 200 Nm. Fig. 8 b shows that the phase of the residual vibration of SFOAM is leading that of FOAM by 0.45 rad, but the amplitude is 24% smaller than that of the latter. We can also see that the displacement of SFOAM is exactly the same (see Fig. 8 b). That is, SFOAM with the first mode reflects the dynamic characteristic of the hub-beam system well, and can be used for controller design.

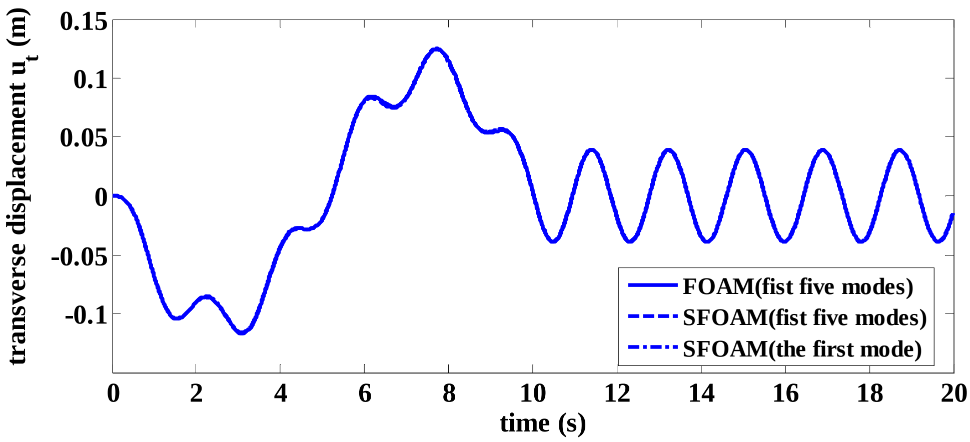

(a) τ_m is 50Nm.

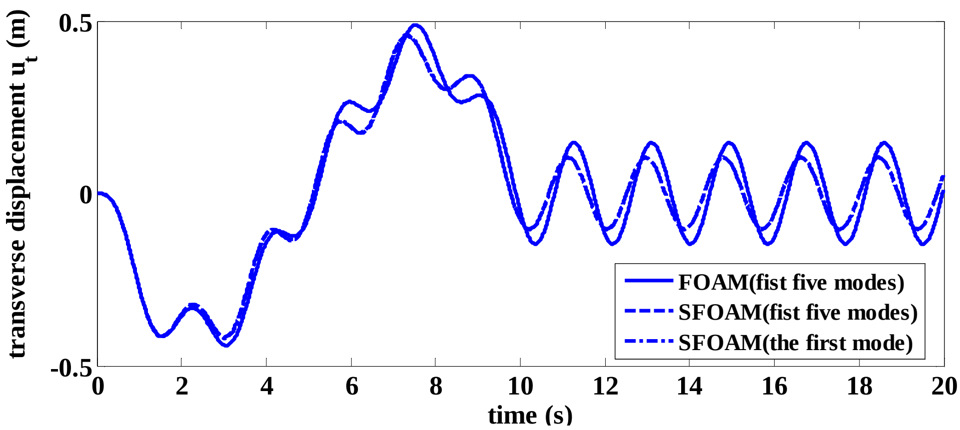

(b) τ_m is 200Nm.

Fig. 8. Tip displacement of the beam when τ_m are 50Nm and 200Nm.

4.4. Vibration Response of Hub-beam System with Tip Mass

The general elastic stiffness matrix of the whole system in TLAM is $\boldsymbol{K}_{22} = \boldsymbol{K}_2 - \dot{\theta}^2 \boldsymbol{M}_2 - m_t \boldsymbol{f}_2^T(l)\boldsymbol{f}_2(l)\dot{\theta}^2$, which shows that the positive definite property of the stiffness matrix in TLAM is determined by the position r_t, the angular velocity $\dot{\theta}$ and the mass m_t. It is known that the positive definite property of $\boldsymbol{K}_{22}$ is determined by the sign of its eigenvalues. Fig. 9 shows this relationship.

As shown in the figure, the critical velocity is 2.91 rad/s when m_t is located on the hub ($l=0$). If the angular velocity exceeds the critical value, the dominant eigenvalues of $\boldsymbol{K}_{22}$ will be negative, which can explain the simulation results shown in Fig. 4 (with 3 rad/s). When the tip mass is located at the tip of the beam, the critical velocities are 2.60 rad/s and 1.91 rad/s for $m_t=0.1$ *kg* and $m_t=0.5$ *kg*, respectively. Fig. 10 shows the transverse displacement of TLAM for the above two cases. For $m_t=0.5$ *kg*, TLAM fails to describe the deformation of the flexible beam when the angular velocity is 2.0 rad/s. However, for the same angular velocity, the simulation result of TLAM is almost the same as for FOAM when $m_t=0$. It is seen that the tip mass decreases the critical angular velocity. Moreover, it can be concluded that as the weight increases, the critical value decreases.

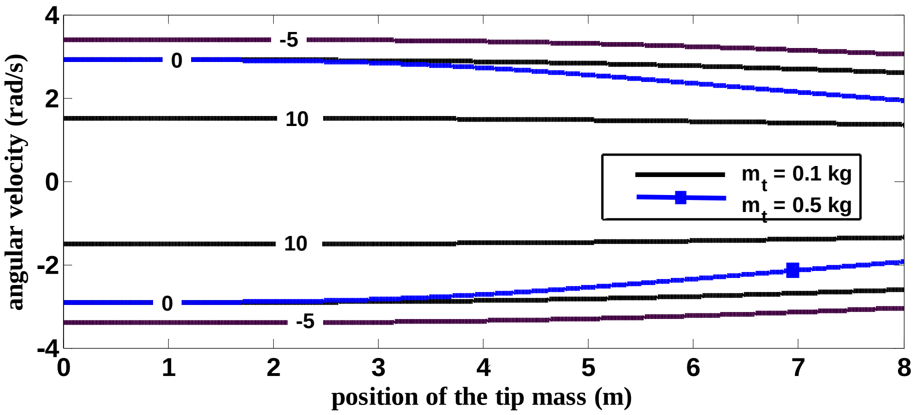

Fig. 9. The dominant eigenvalues of $\boldsymbol{K}_{22}$.

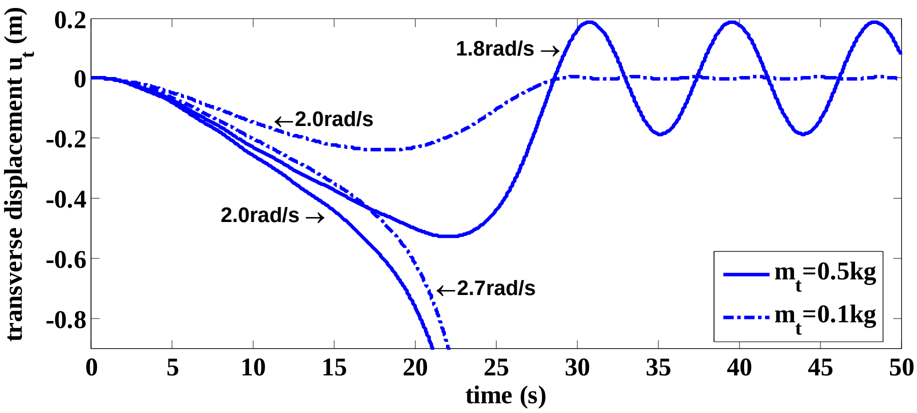

Fig. 10. Response of TLAM system with tip mass.

The generalized elastic stiffness matrix of the tip mass is expressed as $\boldsymbol{K}^{l}_{q_2q_2} = -m_t \boldsymbol{f}_2^T(l)\boldsymbol{f}_2(l)\dot{\theta}^2$, which has a 'softening' effect on the flexible hub–beam system. Because the second order term in coupling deformation is included, the generalized elastic stiffness matrix in FOAM has the term $m_t(r_A+L)\dot{\theta}^2\boldsymbol{S}$, which acts as a 'stiffening' effect.

5. Conclusions

In this paper, the CFOAM, FOAM and SFOAM of a flexible hub–beam system with a tip mass have been presented by using AMM and Lagrangian principle. It is shown that the traditional hybrid co-ordinate approach cannot account for dynamic stiffening and may lead to erroneous results in some high-speed systems. In contrast, the models we developed in this paper can predict valid results. It was also shown that SFOAM model can be used for controller design. The tip mass has a 'softening' effect on the hub-beam system in TLAM, but has a 'stiffening' effect in FOAM. Theoretical analysis and simulation results show that FOAM has better adaptability than TLAM, especially in cases with high rotational speeds. As a future research, experimental investigations on such a system are needed.

Appendix

The coefficients and matrices in the equation of motion of the tip mass are given as follows:

$$M_{\theta\theta}^{l} = m_t\left(r_A + l\right)^2 + m_t\boldsymbol{q}_1^T\boldsymbol{f}_1^T(l)\boldsymbol{f}_1(l)\boldsymbol{q}_1 + m_t\boldsymbol{q}_2^T\boldsymbol{f}_2^T(l)\boldsymbol{f}_2(l)\boldsymbol{q}_2 + 2m_t\left(r_A + L\right)\boldsymbol{f}_1(l)\boldsymbol{q}_1 - m_t\left(r_A + L\right)\boldsymbol{q}_2^T\boldsymbol{S}\boldsymbol{q}_2 \tag{A1}$$

$$\boldsymbol{M}_{q_1\theta}^{l} = \left(\boldsymbol{M}_{\theta q_1}^{l}\right)^T = -m_t\boldsymbol{f}_1^T(l)\boldsymbol{f}_2(l)\boldsymbol{q}_2 \tag{A2}$$

$$\boldsymbol{M}_{\theta q_2}^{l} = \left(\boldsymbol{M}_{q_2\theta}^{l}\right)^T = m_t\left(r_A + L\right)\boldsymbol{f}_2(l) + \boldsymbol{q}_1^T m_t\boldsymbol{f}_1^T(l)\boldsymbol{f}_2(l) \tag{A3}$$

$$\boldsymbol{M}_{q_1q_1}^{l} = m_t\boldsymbol{f}_1^T(l)\boldsymbol{f}_1(l) \tag{A4}$$

$$\boldsymbol{M}_{q_2q_2}^{l} = m_t\boldsymbol{f}_2^T(l)\boldsymbol{f}_2(l) \tag{A5}$$

$$\boldsymbol{G}_{q_1q_2}^{l} = -\left(\boldsymbol{G}_{q_2q_1}^{l}\right)^T = -m_t\boldsymbol{f}_1^T(l)\boldsymbol{f}_2(l) \tag{A6}$$

$$\boldsymbol{K}_{q_1q_1}^{l} = -m_t\boldsymbol{f}_1^T(l)\boldsymbol{f}_1(l)\dot{\theta}^2 \tag{A7}$$

$$\boldsymbol{K}_{q_2q_2}^{l} = -m_t\boldsymbol{f}_2^T(l)\boldsymbol{f}_2(l)\dot{\theta}^2 + m_t\left(r_A + L\right)\dot{\theta}^2\boldsymbol{S} \tag{A8}$$

$$\boldsymbol{Q}_{\theta}^{l} = -\dot{\theta}\left[m_t\boldsymbol{q}_1^T\boldsymbol{f}_1^T(l)\boldsymbol{f}_1(l)\dot{\boldsymbol{q}}_1 + m_t\boldsymbol{q}_2^T\boldsymbol{f}_2^T(l)\boldsymbol{f}_2(l)\dot{\boldsymbol{q}}_2 + m_t\left(r_A + L\right)\boldsymbol{f}_1(l)\dot{\boldsymbol{q}}_1 - m_t\left(r_A + L\right)\boldsymbol{q}_2^T\boldsymbol{S}\dot{\boldsymbol{q}}_2\right] \tag{A9}$$

$$\boldsymbol{Q}_{q_1}^{l} = m_t\left(r_A + L\right)\dot{\theta}^2\boldsymbol{f}_1^T(l) \tag{A10}$$

References

[1]. T. R. Kane, R. R. Ryan, and A. K. Banerjee, Dynamics of a cantilever beam attached to a moving base, *Journal of Guidance, Control, and Dynamics*, Vol. 10, Issue 2, 1987, pp. 139-150.

[2]. R. Jeha, K. Sung-Sup, and K. Sung-Soo, A general approach to stress stiffening effects on flexible multibody dynamic systems, *Mechanics of Structures and Machines*, Vol. 22, Issue 2, 1994, pp. 157-180.

[3]. P. Shi, J. Mcphee, and G. R. Heppler, A deformation field for Euler-Bernoulli beams with applications to flexible multibody dynamics, *Multibody System Dynamics*, Issue 5, 2001, pp. 79-104.

[4]. A. K. Banerjee and J. M. Dickens, Dynamics of an arbitrary flexible body in large rotation and translation, *Journal of Guidance, Control, and Dynamics*, Vol. 13, Issue 2, 1990, pp. 221-227.

[5]. J. Mayo and J. Dominguez, Geometrically nonlinear formulation of flexible multibody systems in terms of beam elements: geometric stiffness, *Computers and Structures*, Vol. 59, 1996, pp. 1039-1050.
[6]. J. Hong and C. You, Advances in dy namics of rigi d-flexible coupling s ystem, *Journal of Dynamics and Control*, Vol. 2, Issue 2, 2004, pp. 1-6, (in Chinese).
[7]. H. Yang, J. Hong, and Z. Yu, Dynamics modeling of a flexible hub-beam system with a tip mass, *Journal of Sound and Vibration*, Vol. 266, Issue 4, 2003, pp. 759-774.
[8]. J. Liu and J. Hong, Geometric stiffening of flexible link system with large overall motion, Computers and Structures, Vol. 81, 2003, pp. 2829-2841.
[9]. J. Jang and D. Li, Research on rigid- flexible coupling d ynamics of spac ecraft with solar panel, *Acta Aeronautica et Astronautica Sinica*, Vol. 27, Issue 3, 2006, pp. 418-422 (in Chinese).
[10]. D. Zhang and Z. Zhu, Dynamic stiffening of rigid-flexible coupling system, *Journal of Nanjing University of Science and Technology*, Vol. 30, Issue 1, 2006, pp. 21-25.